We are IntechOpen,
the world's leading publisher of
Open Access books
Built by scientists, for scientists

6,100
Open access books available

167,000
International authors and editors

185M
Downloads

Our authors are among the

154
Countries delivered to

TOP 1%
most cited scientists

12.2%
Contributors from top 500 universities

CLARIVATE ANALYTICS
BOOK CITATION INDEX
INDEXED

WEB OF SCIENCE™

Selection of our books indexed in the Book Citation Index
in Web of Science™ Core Collection (BKCI)

Interested in publishing with us?
Contact book.department@intechopen.com

Numbers displayed above are based on latest data collected.
For more information visit www.intechopen.com

Chapter

Iterative Technique for Analysis and Design of Circular Leaky-Wave Antenna for the 2.45 GHz RFID Applications

Nizar Sghaier

Abstract

This chapter proposes another scaled-down receiving wire for Radio Frequency Identification uses of 2.45 GHz. Our design comprises of a roundabout microstrip fix radio wire which integrates two concentric annular openings imprinted on multi-facet substrates. The transmission capacity, one of the main qualities of radio wire, can be essentially improved by utilizing a multi-facet dielectric setup. We point by this review to show that the impact of emanating structure stacked by annular rings for the fixed size decrease as well as the benefit of this construction is to make a round-about polarization toward maximal radiation design. The wave idea iterative method is utilized to examine this new radio wire. Utilizing the proposed technique, less figuring time and memory are expected to work out the electromagnetic boundaries of our plan. The approval of the consequences of our created model was checked with realized business programming called "CST Microwave Studio Software" trailed by a trial test. As per the arrived results, we can decide that our new plan radio wire is reasonable for RFID applications in the 2.45 GHz band.

Keywords: RFID, concentric annular slots, multilayer substrates, bandwidth, WCIP, radiation pattern

1. Introduction

The exponential evolution of the need for microwave devices in modern communication systems has prompted manufacturers to invest more and more in this field in order to meet recent market trends. These systems are often multi-band in order to meet several communication standards. Their multiplicity on the same carrier means that more and more attention is being paid to reducing their size. The antenna is one of the essential components in wireless systems for both civil and military applications, space and terrestrial [1–4].

The diversity of the fields of activity using these antennas has increased the need to develop antennas that are agile (in frequency, pattern, or polarization) and multistandard while keeping a compact appearance. The radiation of a circularly

polarized wave is often of interest in order to overcome depolarization phenomena that can occur during propagation [5–8].

In order to meet the various challenges, a multitude of avenues has been explored to adapt to the performance requirements of the applications. Indeed, various topologies and techniques have been investigated in order to meet the required specifications, namely: miniaturization, multi-band operation, and circular polarization radiation while maintaining optimal radio performances (gain, radiation efficiency, reflection coefficient). In addition, a promising way to improve the performance of an antenna is to integrate innovative materials. Many research works have explored this way. Our objective is, therefore, to design miniature microstrip antenna structures for RFID readers in the UHF band with the correct performance [9–11].

Circularly polarized antennas are the most commonly used antennas in RFID communications. In addition, for optimal operation, these antennas must have a particular radiation pattern. It must be omnidirectional in any azimuthal cutting plane, and maintain a high gain, although the choice of a circular antenna is justified by the fact that it has the advantage of being able to achieve circular polarization [12–20].

The rigorous analysis and design of microwave circuits require first of all a rigorous resolution of the equations governing the electromagnetic field, in order to be able to reconstruct the closest to real behavior of the fields in the devices. To satisfy this need, in this chapter, we focus on the study of the circular antenna by the wave concept iterative method (W.C.I.P). This method is based on the manipulation of the incident and reflected waves instead of the electromagnetic field. It is based on the back and forth between the spatial and spectral domains, using the Fourier transform FMT followed by the Hankel transform in the cylindrical coordinate system [21–26].

2. WCIP presentation

2.1 Formulation

To begin, **Figure 1** shows the starting structure.
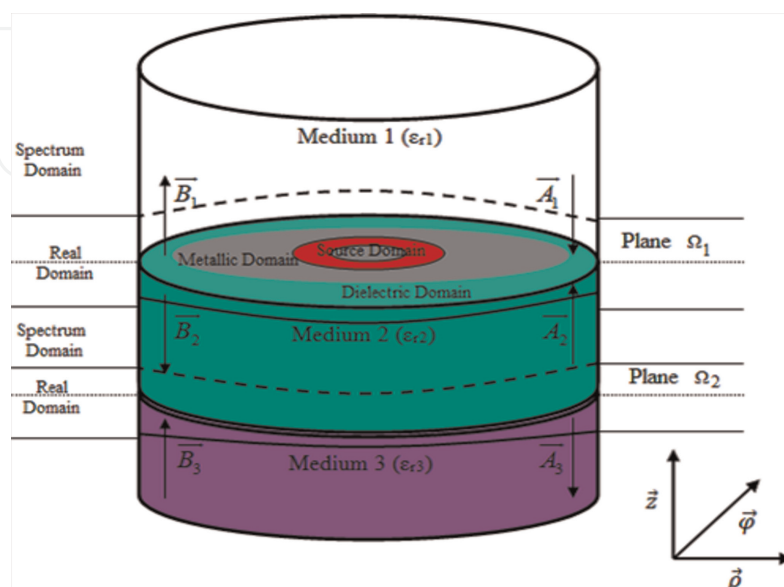
Figure 1.
WCIP structure.

The incident wave and the scattered waves are calculated from the tangential magnetic and electric field at the surface:

$$\begin{bmatrix} A_i \\ B_i \end{bmatrix} = \frac{1}{2\sqrt{Z_{0i}}} \begin{bmatrix} 1 & \sqrt{Z_{0i}} \\ 1 & -\sqrt{Z_{0i}} \end{bmatrix} \begin{bmatrix} E_i \\ J_i \end{bmatrix} \tag{1}$$

Where B_i and A_i are the incident and reflected waves associated with the discontinuity plane Ω_1. Z_{0i} is the characteristic impedance of the medium i (i = 1, 2) given by $Z_{0i} = \sqrt{\mu_0/\varepsilon_0\varepsilon_{ri}}$ (**Figure 2**).

The steps of the iterative method are:

1. Define $\left(\overrightarrow{B_0}\right)$.

2. Calculates $\overrightarrow{B_{\rho,\varphi}} = \Gamma_{\Omega_1}\overrightarrow{A_{\rho,\varphi}} + \overrightarrow{B_0}$

3. Apply HT and FFT: $HT_{/\rho}\left(FFT_{/\varphi}\left(\overrightarrow{B_{\rho,\varphi}}\right)\right) = \overrightarrow{B_{m,n}^{TE,TM}}$

4. Calculates $\overrightarrow{A_{m,n}^{TE,TM}} = \Gamma_i\overrightarrow{B_{m,n}^{TE,TM}}$

5. Apply IHT and IFFT: $HT_{/\rho\text{-}1}\left(FFT_{/\varphi\text{-}1}\left(\overrightarrow{A_{m,n}^{TE,TM}}\right)\right) = \left(\overrightarrow{A_{\rho,\varphi}}\right)$

6. Repeat steps 2 to 5.

$$\begin{cases} E_{/\varphi,\rho}^k = \sqrt{Z_{0i}}\left(A_i^k + B_i^k\right) \\ J_{/\varphi,\rho}^k = \left(A_i^k + B_i^k\right)/\sqrt{Z_{0i}} \end{cases} \tag{2}$$

The expression of return loss at the upper and bottom side of box in the spectrum domain is given by:

$$\hat{\Gamma}_i^{TE,TM} = \frac{1 - Z_{0i}\hat{Y}_{m,n}^{TE,TM}}{1 + Z_{0i}\hat{Y}_{m,n}^{TE,TM}} \tag{3}$$

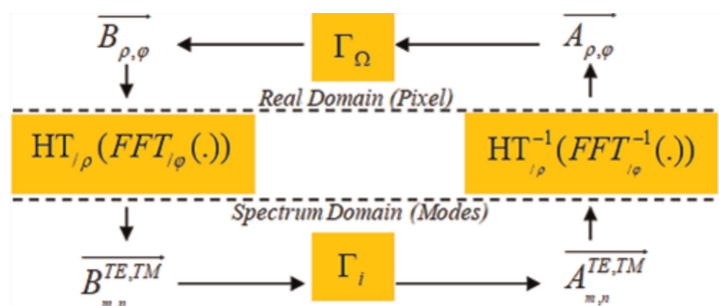Where the admittance $\hat{Y}_{m,n}^{TE,TM}$ is done by **Table 1**:

Figure 2.
WCIP procedure.

	Mode TE	Mode TM
$\hat{Y}_{m,n}^{TE,TM}$	$-jY_r \frac{\gamma}{K_r} \coth(\gamma h)$	$jY_r \frac{K_r}{\gamma} \coth(\gamma h)$

Table 1.
Admittance expressions.

$k_r = \sqrt{\omega^2 \varepsilon_0 \varepsilon_r \mu_0}$, $\gamma = k_\rho^2 - k_r^2$ and $Y_r = \sqrt{\frac{\varepsilon_0 \varepsilon_r}{\mu_0}}$ are the admittance of each domain.

The equivalent circuit of the model is shown in the figure below:
see (**Figure 3**).

The coupling between two layers is characterized by the equivalent admittance Y. The modal admittance seen at the interface Ω_i between layers i-2 and i-1 can be calculated by:

$$Y_{m,n}^{TE,TM}(i-1) = \hat{Y}_{m,n}^{TE,TM}(i-1) \left(\frac{Y_{m,n}^{TE,TM}(i-2) + \hat{Y}_{m,n}^{TE,TM}(i-1) \tanh\left(\gamma_{m,n}^{i-1} h_{i-1}\right)}{\hat{Y}_{m,n}^{TE,TM}(i-1) + Y_{m,n}^{TE,TM}(i-2) \tanh\left(\gamma_{m,n}^{i-1} h_{i-1}\right)} \right), \quad i = 2,3 \tag{4}$$
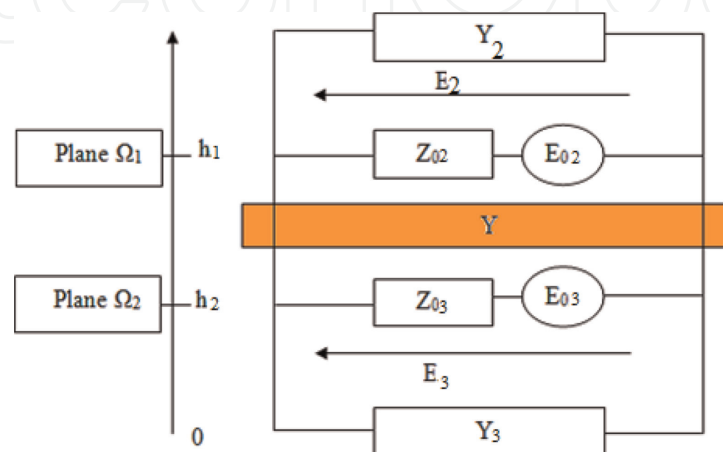
At the printed surface of the discontinuity, the boundary conditions of fields are expressed in terms of waves that consist of three conditions as:

The boundary conditions are given by (5):

$$\begin{cases} E_1 = E_2 = 0 & (Metal) \\ J_1 + J_2 = 0 & (Dielectric) \\ E = E_0 - z_0(J_1 + J_2) & (Source) \end{cases} \tag{5}$$

The relationship between the incident and reflected waves in the spatial domain is given by:

$$B_i = \hat{\Gamma}_\Omega A_i + B_0 \tag{6}$$

Figure 3.
Equivalent circuit of multilayered structure.

With B_0 is the source excitation, the diffraction operator Γ_Ω is defined by:

$$\Gamma_\Omega = \begin{pmatrix} \Gamma_{\Omega 11} & \Gamma_{\Omega 12} \\ \Gamma_{\Omega 21} & \Gamma_{\Omega 22} \end{pmatrix} \tag{7}$$

Where:

$$\begin{cases} \Gamma_{\Omega 11} = -H_m - \dfrac{-1 + n_1 + n_2}{1 + n_1 + n_2} H_s + \dfrac{1 - n^2}{1 + n^2} H_d \\[3mm] \Gamma_{\Omega 12} = \dfrac{2n}{1 + n^2} H_d + \dfrac{2n}{1 + n_1 + n_2} H_s \\[3mm] \Gamma_{\Omega 21} = \dfrac{2n}{1 + n^2} H_d + \dfrac{2n}{1 + n_1 + n_2} H_s \\[3mm] \Gamma_{\Omega 22} = -H_m - \dfrac{-1 - n_1 + n_2}{1 + n_1 + n_2} H_s + \dfrac{1 - n^2}{1 + n^2} H_d \end{cases}$$

Where H is Heaviside function (m: metal; d: dielectric; S: source)

$$\text{And } n = \frac{Z0}{\sqrt{Z_{01} Z_{02}}}, n_1 = \frac{Z_0}{Z_{01}}, n_2 = \frac{Z_0}{Z_{02}}; \tag{8}$$

The passage between the spectral and spatial domain is given by the following **Table 2**:

The radial cut-off constants and normalisation constants for the modes and are given in **Table 3**:

The passage into the spectral domain then requires the transformation of Hankel's incident waves [27]:

The passage into the spectral domain then requires the Hankel transform of the incident waves [7] :

Mode TE	Mode TM
$E_\rho = \frac{e^{j\varphi}}{\sqrt{\pi}} \frac{1}{\Lambda \rho} J_1(\kappa_{\rho m})$	$E_\rho = -j \frac{e^{j\varphi}}{\sqrt{\pi}} \frac{\kappa_{\rho m}}{\Lambda'} J_1'(\kappa_{\rho m}\rho)$
$E_\varphi = j \frac{e^{j\varphi}}{\sqrt{\pi}} \frac{\kappa_{\rho m}}{\Lambda} J_1'(\kappa_{\rho m}\rho)$	$E_\varphi = \frac{e^{j\varphi}}{\sqrt{\pi}} \frac{1}{\Lambda' \rho} J_1(\kappa_{\rho m})$

Table 2.
Standards mode.

	TE and electric wall Or TM and magnetic wall	TM and electric wall Or TE and magnetic wall
$\kappa_{\rho m}$	$J_1(\kappa_\rho a) = 0$	$J_1'(\kappa_\rho a) = 0$
Λ, Λ'	$\Lambda^2 = \frac{1}{2}\kappa_\rho^2 a^2 J_1'^{\,2}(\kappa_{\rho m} a)$	$\Lambda'^2 = \frac{1}{2}\left(\kappa_{\rho m}^2 a^2 - 1\right) J_1^2(\kappa_{\rho m} a)$

Table 3.
Cut-off and modes normalisation.

$$\begin{pmatrix} B^{TE} \\ B^{TM} \end{pmatrix} = \frac{e^{j\varphi}}{\sqrt{2\pi}} \begin{pmatrix} \dfrac{1}{\Lambda\rho}TH_1 & j\dfrac{\kappa_\rho}{\Lambda}TH'_1 \\ -j\dfrac{\kappa'_\rho}{\Lambda'}TH'_1 & \dfrac{1}{\Lambda'\rho}TH_1 \end{pmatrix} \begin{pmatrix} B_\rho \\ B_\varphi \end{pmatrix} \tag{9}$$

With κ and κ′ are the zeros of the Bessel functions and its first-order derivative, and are the normalisation constants of the TE and TM modes respectively and are given by:

$$\begin{cases} TH_1(f(\rho)) = \displaystyle\int_0^a f(\rho)J_1(k_\rho\rho)\rho d\rho \\[4mm] TH_{1'}(f(\rho)) = \displaystyle\int_0^a f(\rho)J_{1'}(k_\rho\rho)\rho d\rho \end{cases} \tag{10}$$

The transition from the spectral domain to the space domain is mandatory. This passage is done by the inverse Hankel transform [7]. We note and respectively follows:

$$\begin{cases} TH_{1-1}(f(\kappa_\rho)) = \displaystyle\int_0^a f(\kappa_\rho)J_1(k_\rho\rho)\kappa_\rho d\kappa_\rho \\[4mm] TH'_{1-1}(f(\kappa_\rho)) = \displaystyle\int_0^a f(\kappa_\rho)J_{1'}(k_\rho\rho)\kappa_\rho d\kappa_\rho \end{cases} \tag{11}$$

The transition to the spatial domain takes the following matrix form:

$$\begin{pmatrix} B_\rho \\ B_\varphi \end{pmatrix} = \frac{e^{j\varphi}}{\sqrt{2\pi}} \begin{pmatrix} TH_1^{-1}\left(\dfrac{1}{\Lambda\rho}\right) & TH'_1{}^{1}\left(j\dfrac{\kappa_\rho}{\Lambda}\right) \\ TH'_1{}^{-1}\left(-j\dfrac{\kappa'_\rho}{\Lambda'}\right) & TH_1^{-1}\left(\dfrac{1}{\Lambda'\rho}\right) \end{pmatrix} \begin{pmatrix} B^{TE} \\ B^{TM} \end{pmatrix} \tag{12}$$

The numerical implementation of the developed method is given by the flowchart below (**Figure 4**):

2.2 Validation

Figure 5 shows the structure of a patch antenna to validate the method which is already developed. This antenna is engraved on a dielectric with relative permittivity $\varepsilon_{r1} = 4{,}25$. The second dielectric is of relative permittivity $\varepsilon_{r2} = 3{,}3$. The dimensions of the patch are given in **Table 4**. We use a discretisation of 100*40 pixels (100 pixels for the radial direction and 40 for the ortho-radial direction).

In order to validate the iterative method, we started first with the comparison of the operation's number between WCIP and MOM which the most used in scientific research [28–30].

The operation number of WCIP is given by:

$$N_{OP} = N(4P + 12\log_2 P) \tag{13}$$

Figure 4.
Flowchart of the WCIP simulation.

Figure 5.
Circular patch excited by a variable source.

Parameter	Value (mm)
Lc	1
Lp	17
Ls	5.4
G	0.8
Hs1	2
Hs2	1

Table 4.
Dimensions of the structure.

The operation number of MOM is given by:

$$N_{OP} = (KP)^3/3 \qquad (14)$$

Where:

- P is the number of meshes

- N is the number of iterations

- K is the proportion of metallic surface in the circuit structure.

Figure 6 shows the number of operations required for WCIP and MOM (**Figure 7**). The convergence of WCIP is completed at 22 iterations as shown in the figure above.

A comparative study is made between the developed method and the MOM method as well as between these two methods and two software CST and HFSS.

Based on **Figure 8**, it can be deduced that the iterative method is the most significant in terms of accuracy.

Table 5 shows the simulation time and memory consumption of each method.
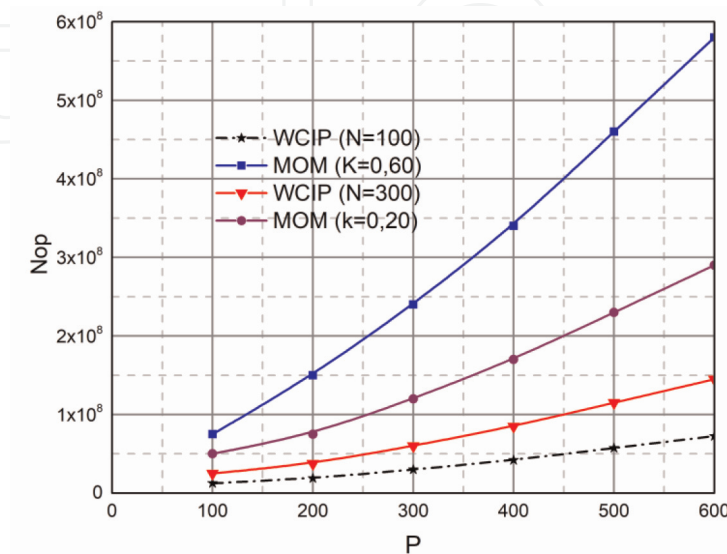
Figure 6.
Operation's number between WCIP and MOM.
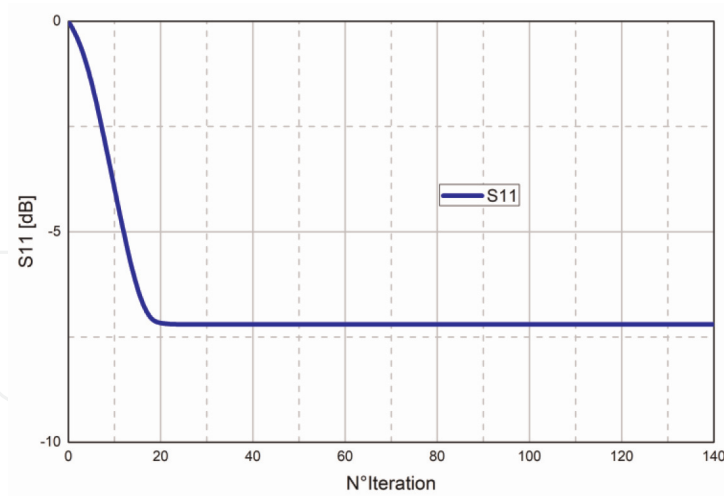
Figure 7.
*Convergence versus iterations number at 2.35 GHz.*
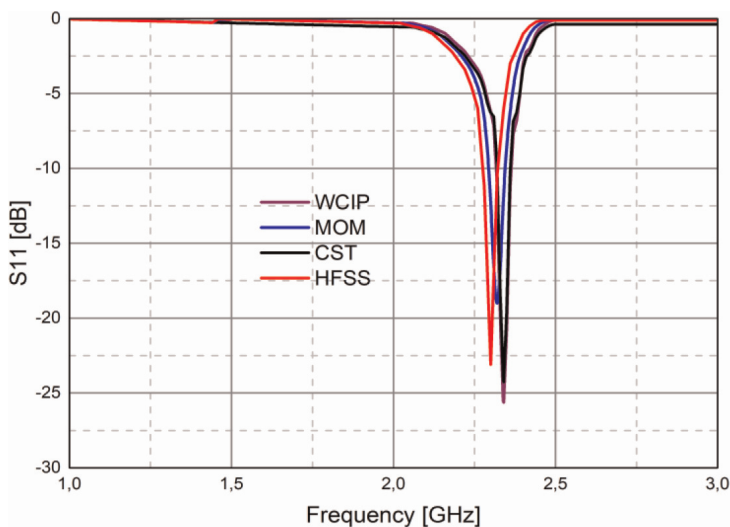
Figure 8.
Simulation return loss using WCIP, MOM, CST and HFSS.

Methods	Response time (s)	Consumption memory (MB)
WCIP	480	450
CST	2100	620
MOM	1756	905
HFSS	629	479

Table 5.
Comparison between these methods.

3. Antenna design

Figure 9 depicts the geometry of the circular leaky-wave antenna. It is characterized by a circular patch of radius Lp = 20 mm which incorporates two concentric annular slots of widths G1 = G2 = 1.058 mm and of successive inner radius R1 = 7.058 mm
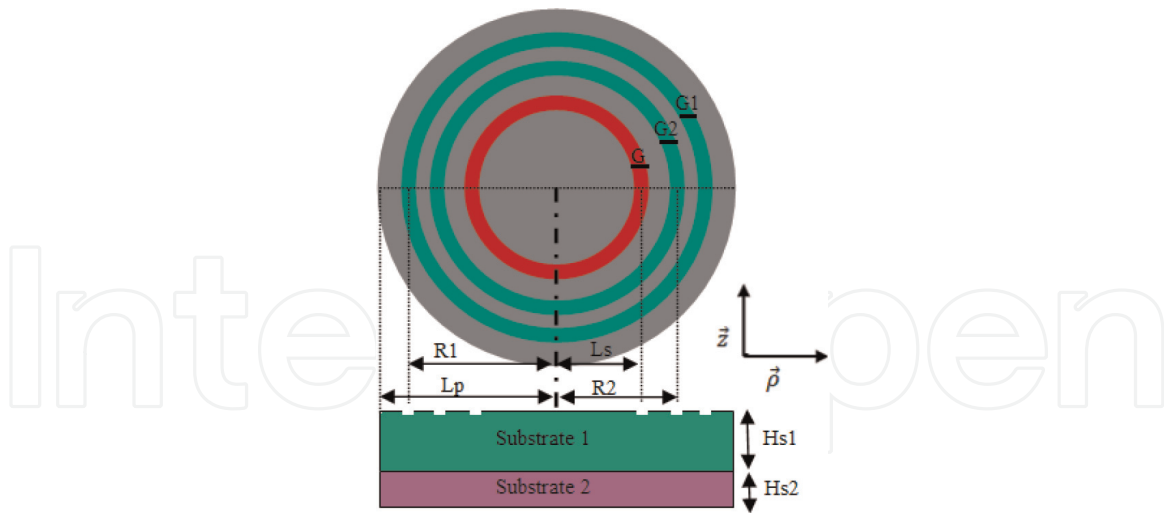
Figure 9.
Antenna design.

and R2 = 12.882 mm is printed on multilayer substrates. The first substrate layer is characterized by a height $H_{s1} = 1$ mm and a permittivity $\varepsilon_{r1} = 4.25$. The parameters $(H_{s2}, \varepsilon_{r2})$ of the second layer will be optimized later. The antenna is supplied by an annular planar source of inner radius Ls = 1.941 mm and of width G = 1.058 mm.

To fix the dimensions of the antenna, a parametric study is necessary. **Figures 10–13** show the variation of the antenna performance as a function of the height of the antenna substrate 2 and its permittivity.

The parametric study shows that the best compromise between gain, efficiency and bandwidth at 2.45 GHz is obtained when $H_{s2} = 0.3$mm and $\varepsilon_{r2} = 2.2$.

4. Results and discussions

The results presented in **Figures 14** and **15** show that the antenna has a resonance peak at the frequency 2.45GHz which corresponds to -38.32 dB with a bandwidth of
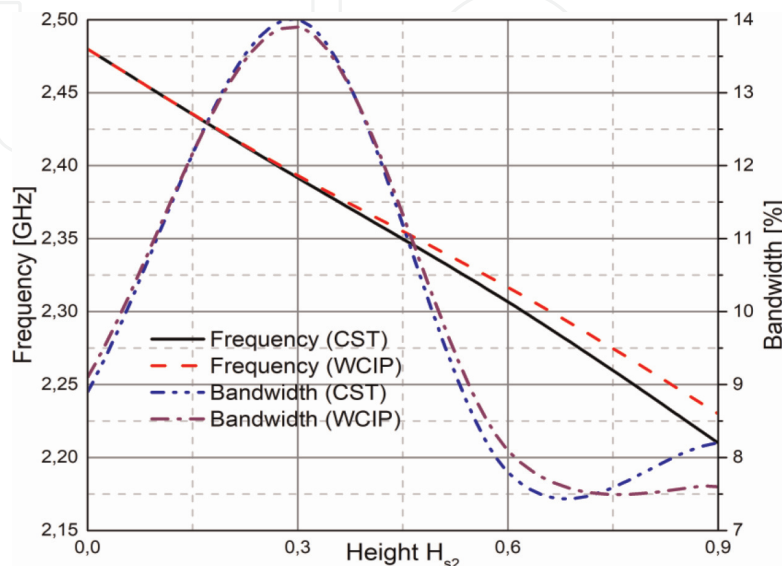
Figure 10.
Simulation frequency and bandwidth for different height of substrate 2 using WCIP and CST.
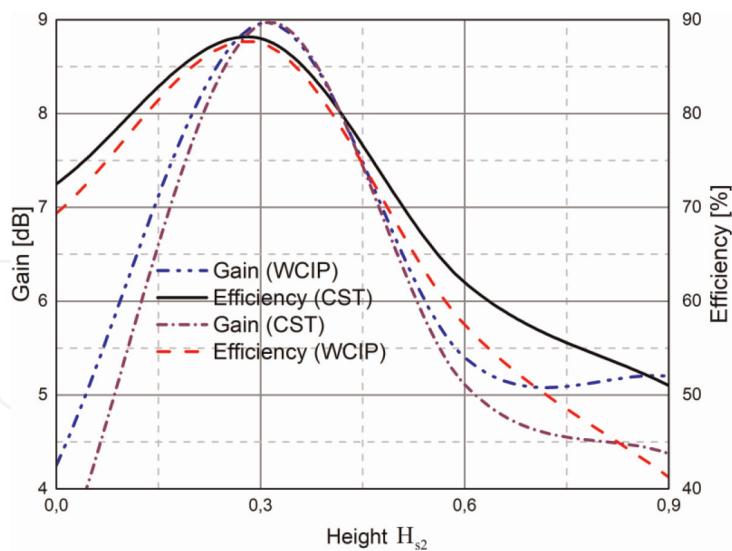
Figure 11.
Simulation gain and efficiency for different height of substrate 2 using WCIP and CST.
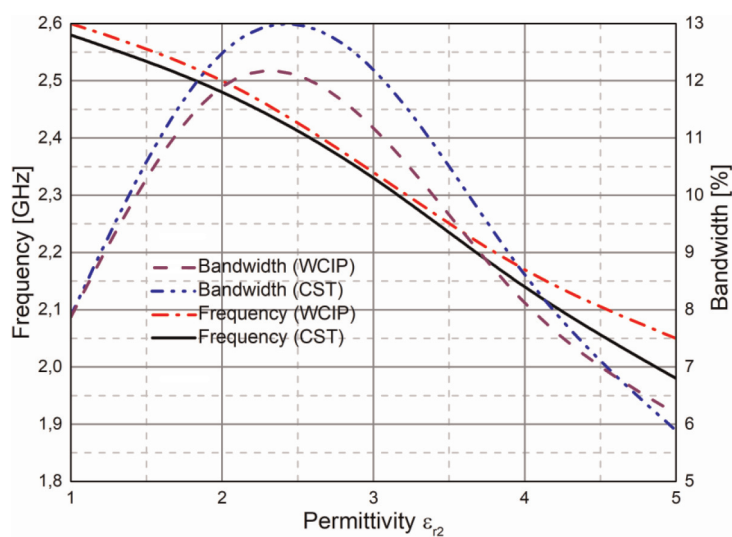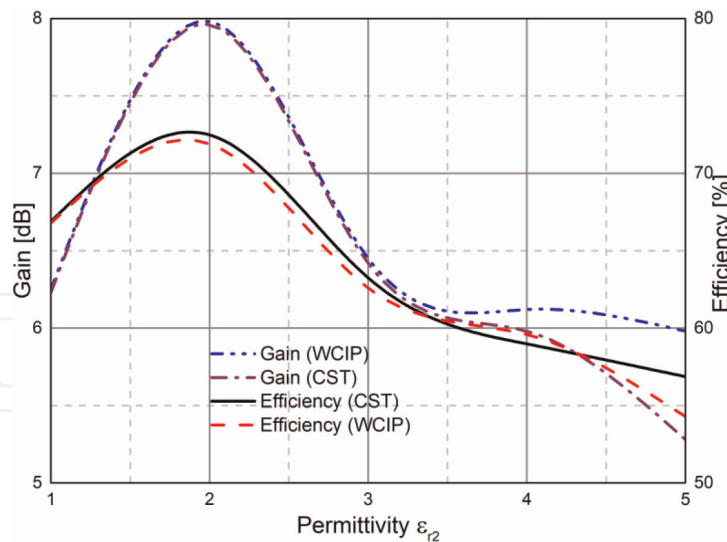

Figure 12.
Simulation frequency and bandwidth for different permittivity of substrate 2 using WCIP and CST.

310MHz (ranging from 2.29 to 2.6GHz) as well as the measured resonance peak is 2.45GHz with –28.57 dB reflection coefficient, which cover the bandwidth of 350MHz (from 2.28 to 2.63GHz). So, the antenna is applicable for RFID applications at 2.45 GHz. In this proposed design, we notice a good agreement between the simulated and measured results.

The measured and simulated radiation patterns at the resonance frequency are given by **Figure 16**. Following the analysis of the results the phi-planes show mostly unidirectional radiation patterns over the specified frequencies.

Figure 16 shows the measured and simulated gain versus the frequency of the proposed antenna. From the simulated results the maximum value of gain is 9.02dB at 2.45GHz as well as the measured value is 8.96dB at 2.45GHz.

The efficiency of the antenna is depicted in **Figure 17**. We obtain a satisfactory value of 88% over a wide frequency bandwidth.

Figure 13.
Simulation gain and efficiency for different permittivity of substrate 2 using WCIP and CST.
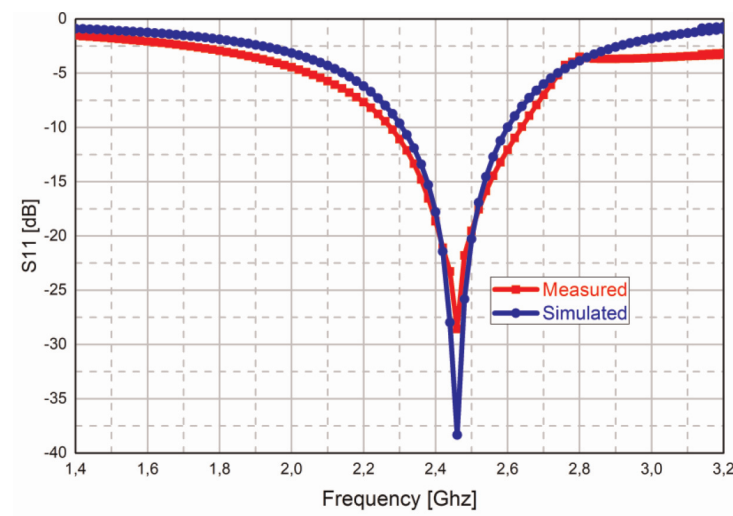
Figure 14.
Simulation and measurement return loss using WCIP.

In free-space, the power received by a tag antenna P_a can be calculated using the Friis free-space [31] equation, where:
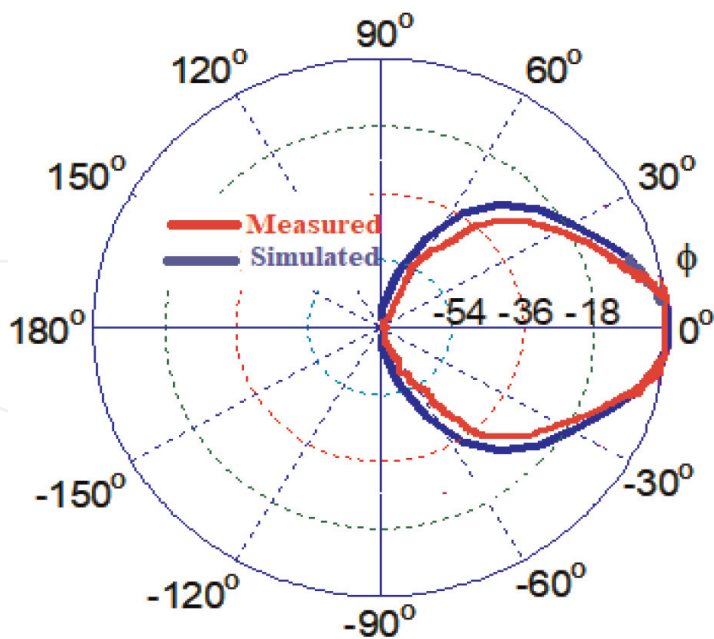
$$P_a = \frac{P_r G_r G_a \lambda^2}{(4\pi)^2 d^2} \qquad (15)$$
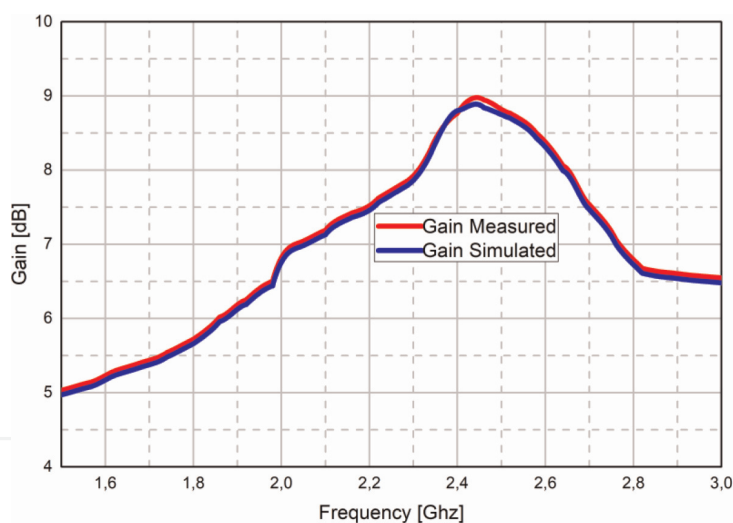
Where (**Table 6**):
The Eq. (16) represents the read range ®:

$$r = \frac{\lambda}{4\pi} \sqrt{\frac{P_r G_r G_a \tau}{P_{th}}} \qquad (16)$$

According to the results of our structure at 2.45 GHz, the numerical values are given in the **Table 7**:
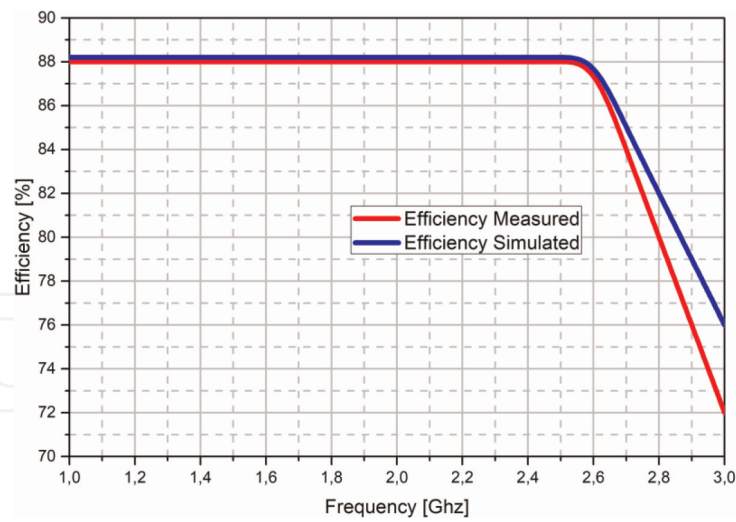
Figure 15.
Simulation and measurement radiation pattern at 2.45 GHz using WCIP.

Figure 16.
Simulation and measurement gain using WCIP.

5. Conclusion

This chapter focuses on the design and production of antennas for radio frequency identification. This technology is experiencing a huge growth and requires the reduction of the cost of an electronic tag to meet the development of its market. Indeed, the reduction of the cost of an RFID tag is a crucial element for the unitary identification of goods. This cost must represent a negligible part compared to the product it identifies. An RFID tag is made of an electronic chip, a support and an antenna. To date, the manufacturing of RFID tags adopts the classic techniques of electronics. A solution for the reduction of the cost of an RFID tag could come from the use of

Figure 17.
Simulation and measurement efficiency using WCIP.

Parameter	Designation
λ	wavelength
P_r	power transmitted
G_r	reader antenna gain
G_a	tag antenna gain
d	distance between the tag and reader

Table 6.
Designation.

Parameter	Values
λ	0.12 m
P_r	1w
τ	0.92
G_a	8.96 dB
P_{th}	0.04 w
G_r	8 dB
r	9.58 m

Table 7.
The numerical values.

printing technologies. The design and realization of RFID tags, especially of their antennas, by using this innovative technology has been demonstrated. In this chapter, we succeeded in designing a miniaturized antenna that meets the requirements of RFID technology.

Author details

Nizar Sghaier
Faculty of Sciences of Tunis, Department of Physics, Tunis EL Manar University,
Tunis, Tunisia

*Address all correspondence to: niizar.sghaier@gmail.com

IntechOpen

References

[1] Byondi FK, Chung Y. Longest-range UHF RFID sensor tag antenna for IoT applied for metal and non-metal objects. Sensors. 2019;**19**(24):5460. DOI: 10.3390/s19245460

[2] Naoui S, Latrach L, Gharsallah A. Metamaterials dipole antenna by using split ring resonators for RFID technology. Microwave and Optical Technology Letters. 2014; **56**(12):2899-2903. DOI: 10.1002/mop.28731

[3] Ziai MA, Batchelor JC. Temporary on-skin passive UHF RFID transfer tag. IEEE Transactions on Antennas and Propagation. 2011;**59**(10):3565-3571. DOI: 10.1109/tap.2011.2163789

[4] Hoon WF, Malek MFBA, Fang LH, Seng LY, Zahid L. On the miniaturization high permittivity DRA with array patches. In: 1st International Conference on Artificial Intelligence, Modelling and Simulation, 03-05 December 2013. Kota Kinabalu, Malaysia: IEEE; 2013. pp. 443-445

[5] Lee B, Harackiewicz FJ. Miniature microstrip antenna with a partially filled high-permittivity substrate. IEEE Transactions on Antennas and Propagation. 2002;**50**(8):1160-1162. DOI: 10.1109/tap.2002.801360

[6] Shi Y, Whites KW. Miniaturization of helical antennas using dielectric loading. In: IEEE-APS Topical Conference on Antennas and Propagation in Wireless Communications (APWC); 03-09 August 2014. Palm Beach, Aruba: IEEE; 2014. pp. 163-166

[7] Porath R. Theory of miniaturized shorting-post microstrip antennas. IEEE Transactions on Antennas and Propagation. 2000;**48**(1):41-47. DOI: 10.1109/8.827384

[8] Ali T, Saadh MAW, Pathan S, Biradar RC. A miniaturized circularly polarized coaxial fed superstrate slot antenna for L-band application. Internet Technology Letters. 2018;**1**(6):e21. DOI: 10.1002/itl2.21

[9] Fan Z, Qiao S, Huang-Fu JT, Ran L-X. A miniaturized printed dipole antenna with V-Shaped ground for 2.45 GHz RFID readers. Progress in Electromagnetics Research. 2007;**71**:149-158. DOI: 10.2528/PIER07022501

[10] He S, Zhang Y, Li L, Lu Y, Zhang Y, Liu H. High performance UHF RFID tag antennas on liquid-filled bottles. Progress In Electromagnetics Research. 2019;**165**:83-92. DOI: 10.2528/PIER19041001

[11] Amin Y, Chen Q, Tenhunen H, Zheng L-R. Performance-optimized quadrate Bowtie RFID antennas for cost-effective and eco-friendly industrial applications. Progress In Electromagnetics Research. 2012;**126**:49-64. DOI: 10.2528/PIER12020805

[12] See KY, Chua EK, Liu Z. Accurate and efficient evaluation of MoM matrix based on a generalized analytical approach. Progress in Electromagnetics Research. 2009;**94**:367-382. DOI: 10.2528/PIER09063002

[13] Jing Y-F, Carpentieri B, Huang T-Z. Experiments with Lanczos Biconjugate a-orthonormalization methods for MoM discretizations of Maxwell's Equations. Progress In Electromagnetics Research. 2009;**99**:427-451. DOI: 10.2528/PIER09101901

[14] Chen M, Zhao X-W, Zhang Y, Liang C-H. Analysis of antenna around

nurbs surface with iterative Mom-Po technique. Journal of Electromagnetic Waves and Applications. 2006;**20**(12): 1667-1680. DOI: 10.1163/ 156939306779292372

[15] De la Rubia V, Zapata J. A methodology for antenna design via the finite element method. In: 2nd European Conference on Antennas and Propagation (EuCAP); 11-16 November 2007. Edinburgh: IET; 2007. pp. 1-10

[16] Sheng X-Q, Yung EKN. Analysis of microstrip antennas on finite chiral substrates. International Journal of RF and Microwave Computer-Aided Engineering. 2003;**14**(1):49-56. DOI: 10.1002/mmce.10115

[17] Dash JC, Jena MR, Mangaraj BB. Analysis of Dipole Antenna and its array using finite element method. 2016 2nd International Conference on Advances in Electrical, Electronics, Information, Communication and Bio-Informatics (AEEICB). 2016. DOI: 10.1109/ aeeicb.2016.7538326

[18] Tirkas PA, Balanis CA. Finite-difference time-domain method for antenna radiation. IEEE Transactions on Antennas and Propagation. 1992;**40**(3): 334-340. DOI: 10.1109/8.135478

[19] Lampe B, Holliger K, Green AG. A finite-difference time-domain simulation tool for ground-penetrating radar antennas. Geophysics. 2003;**68**(3): 971-987. DOI: 10.1190/1.1581069

[20] Houaneb Z, Zairi H, Gharsallah A, Baudrand H. Modeling of cylindrical resonators by wave concept iterative process in cylindrical coordinates. International Journal of Numerical Modelling: Electronic Networks, Devices and Fields. 2011;**24**(2):123-131. DOI: 10.1002/jnm.765

[21] Gharsallah A, Mami A, Douma R, Gharbi A, Baudrand H. Analysis of a microstrip antenna with fractal multilayer substrate using iterative method. International Journal of RF and Microwave Computer-Aided Engineering. 2001;**11**(4):212-218. DOI: 10.1002/mmce.1026

[22] Richalot E, Wong MF, Baudrand H, Fouad-Hanna V. An iterative method for modeling of antennas. International Journal of RF and Microwave Computer-Aided Engineering. 2001;**11**(4):194-201. DOI: 10.1002/ mmce.1024

[23] Djouimaa A, Titaouine M, Adoui I, et al. Tunable FSS simulation using WCIP method for multiband and dual polarized applications. Radioelectronics and Communications Systems. 2017;**60**: 106-112. DOI: 10.3103/S073527271 7030025

[24] Cassivi Y, Wu K. Substrate integrated nonradiative dielectric waveguide. IEEE Microwave and Wireless Components Letters. March 2004;**14**(3):89-91. DOI: 10.1109/ LMWC.2004.824808

[25] Baudrand H, Titaouine M, Raveu N, Fontgland G. Electromagnetic modeling of planar almost periodic structures. In: SBMO/IEEE MTT-S International Microwave and Optoelectronics Conference (IMOC); 03-06 November 2009. Belem, Brazil: IEEE; 2009. pp. 427-431

[26] Ammar N, Baudrand H. Wave concept iterative process method for multiple loop antennas around a spherical media. IET Microwaves, Antennas and Propagation. 2019;**13**: 666-674. DOI: 10.1049/iet-map.2018. 5661

[27] Hlali A, Houaneb Z, Zairi H. Dual-band reconfigurable graphene-based

patch antenna in terahertz band: Design,
analysis and modeling using WCIP
method. Progress in Electromagnetics
Research C. 2018;**87**:213-226.
DOI: 10.2528/PIERC18080107

[28] Liu Z-L, Wang C-F. Mutual coupling
analysis of multiple on-board antennas
with sub-domain MoM-PO method. In:
IEEE International Symposium on
Electromagnetic Compatibility and 2018
IEEE Asia-Pacific Symposium on
Electromagnetic Compatibility (EMC/
APEMC); 14-18 May 2018. Suntec City,
Singapore: IEEE; 2018. p. 89

[29] Latifa NB, Aguili T. Synthesis and
optimization of almost periodic antennas
using Floquet modal analysis and MoM-
GEC method. Journal of Electromagnetic
Analysis and Applications. 2019;**11**:1-16.
DOI: 10.4236/jemaa.2019.111001

[30] Pereira-Filho OMC, Barbosa HB,
Diniz CA, Tinoco-S AF. Method of
moments analysis of arrays of cylindrical
microstrip antennas with superstrate.
IET Microwaves, Antennas and
Propagation. 2018;**12**(4):561-568.
DOI: 10.1049/iet-map.2016.0986

[31] Shi Y, Qi K, Liang C-H. A
miniaturized design of 2.45-GHz RFID
tag antenna. Microwave and Optical
Technology Letters. 2015;**57**(8):
1905-1908. DOI: 10.1002/mop.29223